

Voltage Clamp Simulations for Multifiber Bundles in a Double Sucrose Gap: Cable Complications

K. SOLCHENBACH¹, H. G. HAAS² and G. BROMMUNDT²

1 *Institute for Foundations of Information Technology, Gesellschaft für Mathematik und Datenverarbeitung, D 5205 St. Augustin, Federal Republic of Germany*

2 *Second Institute of Physiology, University of Bonn, Wilhelmstrasse 31, D 5300 Bonn, Federal Republic of Germany*

Abstract. A theoretical model is presented for voltage clamp of a bundle of cylindrical excitable cells in a double sucrose gap. The preparation in the test node is represented by a single one-dimensional cable (length/diameter ratio ≈ 30) with standard Hodgkin-Huxley kinetics for transmembrane Na current. Imperfections of voltage control due to internal (longitudinal) resistivity and external (radial) resistance in series to the membrane are analysed. The electrical behavior of a fiber is described by the cable equation with appropriate boundary conditions and subsidiary equations reflecting the membrane characteristics. Membrane voltage and current distribution in response to a step command was obtained by numerical integration. The results are described in two papers. The present paper deals with the effect of internal resistivity with the external resistance being neglected. The closed loop response of a fiber displays a strong tendency to oscillate. To stabilize the system a phase lead was inserted and the gain of the control amplifier was reduced. Conditions for stability were examined by Nyquist analysis. When the Na system was activated by a command pulse below E_{Na} , a voltage gradient developed between a depolarization (relative to the command signal) at the end where voltage was monitored and a hyperpolarization at the site of current injection. In spite of a poor voltage control the total measured current appeared to have a smooth transient. With large voltage gradients a small, second inward current was seen. At a low (high) Na conductance maximum peak inward current was larger (smaller) than the current expected from ideal space clamping.

Key words: Sucrose gap — Voltage clamp — Na current — Cable complications — Computer simulation

Introduction

Voltage clamping of multicellular preparations (e.g. cardiac or smooth muscle bundles) is subject to a number of experimental errors resulting from the

three-dimensional structure of the tissue. When a current is injected into a cylindrical bundle made up of hundreds of thin, parallel-aligned, interconnected fibers and is collected by an external electrode, it has to pass a complicated resistive network inside the bundle. The main components of the network are i) a longitudinal resistance to intracellular current flow (including the resistance of cell-to-cell junctions) and ii) a radial resistance to extracellular current (in particular the resistance of intercellular clefts and of an endothelial layer surrounding the bundle). Both factors result in inhomogeneities of the voltage and current distribution in the bundle, thus preventing a proper space clamp (cf. Johnson and Lieberman 1971; Kootsey and Johnson 1972; McGuigan 1974; Tarr and Trank 1974; Moore et al. 1975; Ramón et al. 1975; Attwell and Cohen 1977; Beeler and McGuigan 1978; Haas and Brommundt 1980; Fischmeister et al. 1982). In detail, the effects of intra- and extracellular resistances will depend on the position of current and voltage electrodes. With a double sucrose gap apparatus, current is applied at one end of the test node (I-end) and voltage is monitored at the opposite end (V-end). In this arrangement a strict voltage control is expected only for the V-end of the superficial fibers of a bundle. Regarding the fibers as one-dimensional cables with a marked axial resistance, the clamp current will create a longitudinal voltage gradient. The membrane potential at the I-end deviates in the hyperpolarizing (depolarizing) direction from the potential at the V-end when current is withdrawn from (injected into) a fiber, i.e., during the phase of transmembrane inward (outward) current flow (Moore et al. 1975). Thus the driving force for both inward and outward current is increased at the I-end of a fiber as compared to the monitored end. On the other hand, an extracellular series resistance causes a radial voltage drop that shifts the membrane potential of the inner fibers in opposite direction, i.e. from the command signal to a more positive (negative) level during inward (outward) current flow, so that the driving force for transmembrane current is decreased. Thus the fibers of a bundle are affected in a dual fashion and the two effects might abolish each other to some extent (Ramón et al. 1975).

In this and a following paper voltage clamp simulations are presented for an active fiber bundle in a double sucrose gap. The bundle is modelled by a single fiber with appropriate values of internal (longitudinal) and external (radial) resistance and an excitable membrane with standard Hodgkin—Huxley (1952) sodium channels. The voltage profile in the test gap is described by a set of differential equations which are solved by numerical methods. Membrane Na conductance, internal and external resistances are set to various levels in order to illustrate their effects on the distortion of fast inward current. The present paper deals with the general properties of the voltage clamp circuit and with the influence of a longitudinal resistance in the absence of a series resistance. In a following paper (Haas et al. 1987) the effects of longitudinal and radial resistance shall be described in conjunction.

The theoretical model

The voltage clamp circuit

Consider a single fiber (a one-dimensional cable) in a conventional double sucrose gap voltage clamp arrangement (Fig. 1). The test node is flanked by two sucrose streams acting as high-resistance partitions between the central compartment (perfused with test solution) and the side pools (filled with isosmotic KCl solution in order to establish a membrane potential near zero value and a low membrane resistance at the ends of the fiber). Interdiffusion of saline and sucrose at the boundaries between adjacent pools is ignored. A minimum node length of several hundred microns is required for the perfusion to be stable. Extracellular gross electrodes are used for current application and voltage recording. When a command pulse is applied to the control amplifier, current is injected into the left side pool, it enters the end of the fiber, crosses the membrane of the test segment, and is collected by the central electrode which is kept at ground potential. Membrane potential at the far end is recorded across the right sucrose gap and fed back to the amplifier. Assuming a thin fiber with a space constant comparable to, or shorter than, the length of the test node, a voltage drop along the fiber will arise and voltage control (if realizable at all) is confined to the right border of the test node. The stability of the voltage clamp circuit is critical and an abrupt perturbation of the system may induce increasing oscillations. This is mainly due to a delay in the spread of potential along the test node. In a closed loop configuration this delay appears as a phase lag which (together with a lag of the transient response of the control amplifier) exceeds 180° at high frequencies, so that the negative feedback is converted into a positive one. Thus the system will go into oscillation unless the gain along the feedback loop is below unity at the critical frequency range.

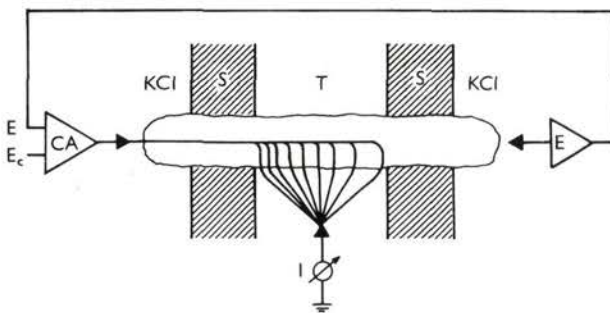


Fig. 1. Diagram (not to scale) of a fiber in a double sucrose gap voltage clamp apparatus as designed by Julian et al. (1962a, b). S: sucrose partitions; T: test compartment; CA: control amplifier; E_c : command signal; E: voltage recording device; I: operational amplifier in currentometric mode. Steady membrane current density decreases with increasing distance from the left sucrose partition.

The arrangement shown in Fig. 1 is oversimplified since a perfect external insulation by sucrose is assumed and the extracellular space of the test node is taken as a volume conductor of zero resistance. A more realistic representation is shown in Fig. 2, with an external leak across the sucrose gap (R_{sb}) in parallel to the internal resistance of the fiber (R_{ax}) in the sucrose region and an extracellular resistance in series to the membrane of the test node. The latter reflects an impediment to current flow between cell membrane and collecting electrode. For simplicity, the extracellular pathway is lumped into a single resistor (R_s). A sucrose gap leak has a short-circuiting effect on both current and voltage measurement.

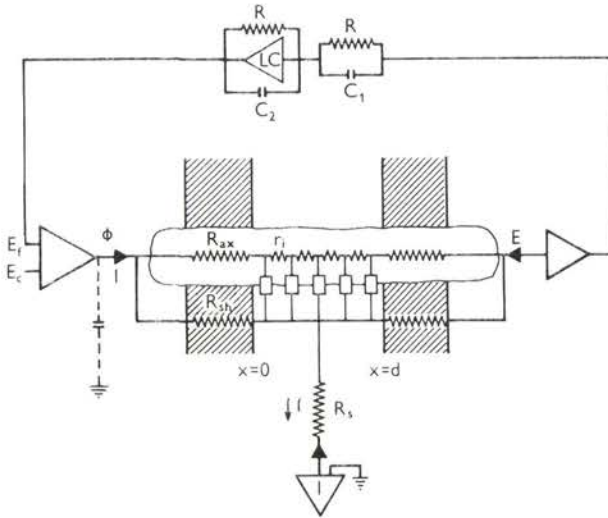


Fig. 2. Voltage clamp circuit for a fiber in a double sucrose gap including access resistance R_{ax} , sucrose leakage resistance R_{sb} , and lumped series resistance R_s . Several segments of the fiber membrane in the test node are represented by rectangles symbolizing membrane capacitance in parallel with membrane channels and the respective ionic batteries. Internal longitudinal resistance r_i is distributed between the segments. On both ends of the preparation part of the controlling current flows to ground via the shunt pathways. Transgap voltage is recorded by a high input impedance inverting amplifier, passed through an amplifier (LC) providing lead compensation, and fed back to the negative input of the control amplifier. The compensating amplifier is designed as a combined differentiator and integrator. Differentiation alone would give a phase lead up to 90° and an undesired increase in amplitude with high frequencies. This is counteracted by integration. Phase lead by the combined device requires $R_1 C_1 > R_2 C_2$. To have unity gain in a steady state, $R_1 = R_2 = R$. Phase lead is maximal at a frequency of $1/(2\pi\sqrt{\tau_1\tau_2})$ and reaches the value $\text{arctg}(\tau_1 - \tau_2)/(2\sqrt{\tau_1\tau_2}) < 90^\circ$. For very low or high frequencies, phase lead tends to zero. The gain is ≈ 1 at low frequencies and approaches τ_1/τ_2 in the high frequency range.

The current (I) injected into the left pool is split into two components, one of which flows past the preparation to ground. Similarly some current is lost between the

right pool and the central compartment, and the potential measured across the right gap is reduced as compared with the actual transmembrane potential by the factor $R_{sh}/(R_{sh} + R_{ax})$. The isolation factor may be 0.9 or more under suitable conditions. (A modification of the model accounting for a distributed nature of sucrose gap leakage is described in Appendix to the subsequent paper). In the presence of a series resistance, the parameter being controlled is not the membrane potential itself but the sum of membrane potential plus the voltage drop across the series resistance (IR_s). An external resistance has a stabilizing effect on the feedback circuit since it decreases the phase lag along the test node. Stability is further increased when a series resistance occurs in combination with a shunt resistance. As an active stabilizing element a lead compensation based on an inverter and an analog mode amplifier with appropriate input and feedback impedances was inserted into the feedback path.

Quantitatively, the electrical behavior of the fiber in the test node is described by the cable equation

$$\partial^2 V_m / \partial x^2 = (2R_i/a)(C_m \partial V_m / \partial t + I_{ion}) \quad (1)$$

where V_m is the transmembrane potential as a function of distance (x) and time (t) and the other symbols have their usual meanings (see Table 1). The term I_{ion} is related to V_m and t by auxiliary equations depending on the membrane characteristics, e.g. ordinary differential equations of the Hodgkin and Huxley (H-H) (1952) type. Any particular solution of eq. (1) is determined by the boundary conditions and the initial condition for $V_m(x, t)$. The boundary conditions (based on continuity of longitudinal internal current flow at the boundaries between sucrose and test solution) are

$$\partial V_m / \partial x_{(x=d-0)} = -V_d q / b \quad (2)$$

$$\partial V_m / \partial x_{(x=0+0)} = V_o q / b - IR_p / b \quad (3)$$

where V_d and V_o are the membrane potentials at the ends of the test node, and $q = R_{ax}/(R_{sh} + R_{ax})$. According to Kirchhoff's law the clamp current is

$$I = \frac{\Phi - V_o(1-q)}{R_p + R_s} \quad (4)$$

Thus eq. (3) can be rewritten

$$\partial V_m / \partial x_{(x=0+0)} = \frac{V_o(R_p + qR_s) - \Phi R_p}{b(R_p + R_s)} \quad (3a)$$

The numerical values of I or Φ at a time t follow from the feedback configuration. The electronics of the voltage clamp circuit shown in Fig. 2 is described by the

following equations: Assuming a single time constant control amplifier, the relation between output voltage Φ and net input voltage, $E_m = E_c - E_t$, is

$$(E_c - E_t)G = \Phi + \tau d\Phi/dt \quad (5)$$

where G is the d.c. gain of the amplifier. The signal E_t is correlated to E , the potential of the right-hand side pool, by

$$E_t + \tau_2 dE_t/dt = E + \tau_1 dE/dt \quad (6)$$

Furthermore

$$E = IR_s + V_d(1 - q) \quad (7)$$

The ionic current flow across the fiber membrane is assumed to be carried by sodium and potassium ions. For simplicity the potassium conductance (g_K) is taken to be constant. The Hodgkin—Huxley (1952) formulation was used to describe the sodium conductance (g_{Na}) as a function of voltage and time, with the only modification that the sign of membrane potential and current has been inverted as compared to the original notation.

The control amplifier was chosen to produce a relatively low gain and long response time (i.e. a low gain-bandwidth product) in order to avoid oscillations. For commercial operational amplifiers a gain-bandwidth product of 1 MHz is a typical value. This means a time constant of about 0.16 ms when the d.c. gain is adjusted to 1000. A 6-fold reduction of the gain-bandwidth product (which is easily achieved e.g. by application of a capacitive element across the amplifier output) would give a time constant $\tau \approx 1$ ms at $G = 1000$. Those parameters were used in the simulations with a high series resistance which shall be described in the following paper (Haas et al. 1987). Lower values of G were needed for the calculations with $R_s = 0$ presented in this paper (see below). The ratio of G/τ was kept constant throughout the study. Maximum output voltage of the control amplifier was taken to be ± 10 V.

The stability problem

The feedback circuit is most liable to oscillate in response to a step command when the external series resistance (R_s) is at zero level. For a passive cable with a radius $a = 3 \times 10^{-4}$ cm, membrane resistance $R_m = 2 \text{ k}\Omega\text{cm}^2$, and a core resistivity $R_i = 200 \text{ }\Omega\text{cm}$, the length constant $\lambda = \sqrt{aR_m/(2R_i)}$ reaches 0.038 cm which is about twice the length of the test node. When the gain of the control amplifier is set to $G = 1000$ the response to a step input is a full scale oscillation, with the output voltage of the control amplifier alternating between ± 10 V. Oscillation is unavoidable unless the open loop gain of the system is less than one at the frequency

where the total phase lag reaches 180° . The easiest way to stabilize the system is to reduce the gain factor of the control amplifier (which is, of course, at an expense of the accuracy of steady state control) and/or to introduce a phase lead. This is illustrated in Fig. 3. With $G = 100$ and no phase lead, the system is still unstable and the step response at the point of voltage recording is an increasing oscillation with a frequency of about 1100/s (A). By setting the time constants of the compensating amplifier to appropriate values oscillation is converted into a transient ringing which fades out within 3 ms and the frequency is increased to 1450/s (B). Upon reducing the control amplifier gain to $G = 50$ and using the same

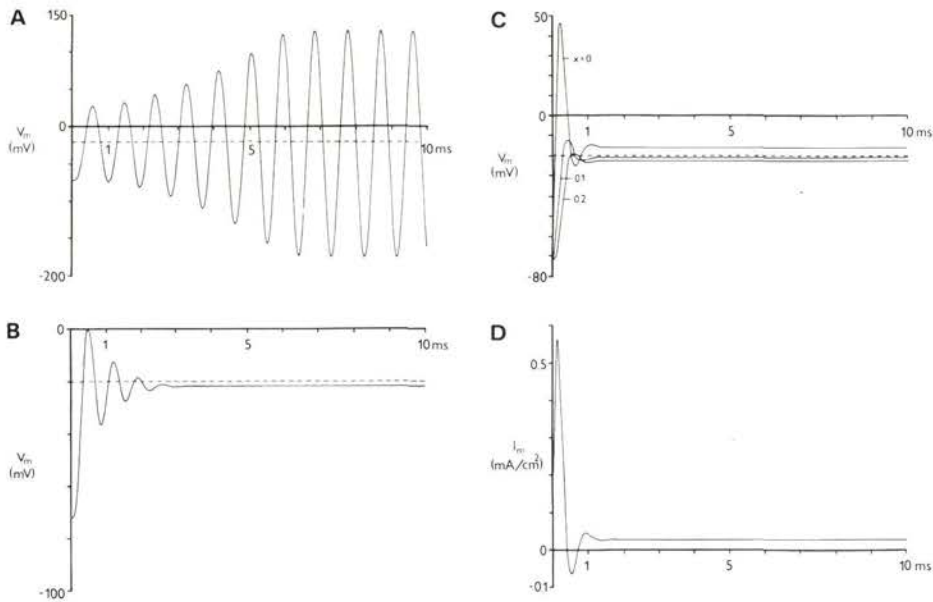


Fig. 3. Step responses of a passive RC cable with a length/diameter ratio of 33 obtained with the double sucrose gap voltage clamp arrangement as in Fig. 2 in the absence of an external series resistance. Sodium conductance of fiber membrane was set to zero while $g_K = 0.5 \text{ mS/cm}^2$. The command pulse was a depolarization from -72 mV (near the resting state) to -20 mV (interrupted horizontal line). Abscissa: time after onset of clamp. The curves represent the time courses of membrane potential (A–C) and of clamp current (D) with different electronic arrangements. Voltage recordings refer to the right end of the test node ($x = 0.2 \text{ mm}$) in (A) and (B) and to three positions (left end, middle, and right end of the node) in (C). Clamp current is expressed as mean membrane current density, I_m , of the test node, neglecting current losses in the sucrose gap regions. The parameters used for the control amplifier and the compensating amplifier were $G = 100$, $\tau = 0.1 \text{ ms}$, $\tau_1 = \tau_2 = 0$ in (A); $G = 100$, $\tau = 0.1$, $\tau_1 = 0.1$, $\tau_2 = 0.01 \text{ ms}$ in (B); $G = 50$, $\tau = 0.05$, $\tau_1 = 0.1$, $\tau_2 = 0.01 \text{ ms}$ in (C) and (D). With the values of τ_1 and τ_2 used in (B–D), a phase lead of 55° is reached at frequencies around 5000 Hz (cf. legend to Fig. 2).

phase lead arrangement the transient voltage response to a step command changes from light to strong damping, and ringing is restricted to about one cycle (*C*). We consider this the optimum correction to be achieved by simple procedures. The first half of the cycle appears as a depolarizing "overshoot" relative to the steady potential. The transient response travels along the test node in the manner of a decremental wave. The overshoot reaches large positive potentials at the I-end but is only a few mV at the V-end. The steady potential distribution shows the expected depolarization of the I-end compared to the V-end. The steady value of V_d differs from the command level by about 2.5 mV because of the low gain of the control amplifier and an imperfect external insulation in the sucrose gap region (cf. eq. (5a) in the Results section). The clamp current record (*D*) shows a transient response which leads the voltage responses seen in (*C*).

Theoretically, the conditions for stability can be stated by determining the transfer function of the open loop system and referring to the Nyquist criterion (see Appendix). This procedure, however, is meaningful only for the case of a passive RC cable. The problem is much more complicated in the case of an active cable. Not only the general reduction of membrane resistance during the phase of excitatory inward current, but also the transient kinetics of the Na system favors permanent or increasing oscillations.

Specification of parameters

In the present work, the following parameters were set to fixed values: Fiber radius, $a = 3 \times 10^{-4}$ cm (this value is typical e.g. of frog atrial fibers, cf. Haas et al. 1983); sucrose gap width, $b = 0.14$ cm; test node length, $d = 0.02$ cm; membrane potassium conductance, $g_K = 0.5$ mS/cm²; membrane specific capacitance, $C_m = 2$ μ F/cm². Internal resistivity, R_i , was 200 Ω cm, corresponding to a resistance per unit length of fiber, $r_i = 0.708 \times 10^9$ Ω /cm. Shunt resistance, R_{sh} , was assumed to be $20 \times R_{ax}$ so that $q = R_{ax}/(R_{sh} + R_{ax}) = 0.0476$. External resistance, R_s , was taken to be zero. In the computations with an active fiber maximum sodium conductance, \bar{g}_{Na} , was 10, 50 or 120 mS/cm². The d.c. gain of the control amplifier was set to $G = 50$; amplifier time constant was $\tau = 0.05$ ms. The time constants of the compensating amplifier were chosen to be 0.1 and 0.01 ms, respectively. The Na and K equilibrium potentials were taken as 43 and -74.5 mV, respectively. All computations are referred to an initial membrane potential of -72 mV which is close to the different resting levels resulting from variation of \bar{g}_{Na} . Initial values of the Hodgkin—Huxley variables are $m_\infty = 0.053$; $h_\infty = 0.6$.

Numerical methods

For spatial discretization of eqs. (1, 2, 3a) the interval $[0, d]$ is subdivided into N equidistant subintervals by the gridpoints $x_i = ih$ with $i = 0, \dots, N$; $h = d/N$. The

differential operator $\partial^2/\partial x^2$ is replaced by the usual 3-point second order difference operator

$$\frac{\partial^2 V}{\partial x^2}(x_i) = \frac{1}{h^2} (V_{i+1} - 2V_i + V_{i-1}) + O(h^2) \quad (8)$$

where $V_i = V_m(x_i, t)$. The boundary conditions are discretized by using central second order differences, involving the fictitious points x_{-1} and x_{N+1} . Replacing the differential operators in eqs. (1, 2, 3a) by the difference operators we obtain for $i = 0, \dots, N$; $t > 0$ the relations

$$\frac{dV_i}{dt} = \frac{a}{2R_i C_m h^2} (V_{i+1} - 2V_i + V_{i-1}) + I_{ion}(x_i, t)/C_m \quad (9a)$$

$$(V_1 - V_{-1})/2h = c_1 V_0 + c_2 \Phi \quad (9b)$$

$$(V_{N+1} - V_{N-1})/2h = c_3 V_N \quad (9c)$$

with the abbreviations $c_1 = (R_p + qR_s)/\{b(R_p + R_s)\}$; $c_2 = -R_p/\{b(R_p + R_s)\}$; $c_3 = -q/b$. Application of eq. (8) at points x_0 and x_N allows us to eliminate the fictitious points.

For time discretization we rewrite eq. (6) introducing a new variable $E_1 = \tau_2 E_t - \tau_1 E$

$$dE_1/dt = -E_1/\tau_2 + (1 - \tau_1/\tau_2)E; \quad E_1(0) = 0 \quad (6a)$$

By combining the ordinary differential equations (ODEs) (5, 6a) and the H-H equations with eqs. (9a—c) we obtain a nonlinear stiff system of ODEs for the unknowns $V_0, \dots, V_N, E_1, \Phi, m_0, \dots, m_N, h_0, \dots, h_N$ with certain initial conditions at $t = 0$.

This system is discretized implicitly using either the method of Crank-Nicolson (CN) (1947) or the implicit Euler method. The CN-scheme is absolutely stable (A-stable), with no restriction on the relative sizes of temporal and spatial steps. Thus artificial oscillatory components in the initial phase of the solution which are generated by numerical errors are not amplified. A-stability is sufficient if the artificial components are small relative to the components of the "true" solution. This condition is satisfied when an appreciable series resistance is included in the single fiber model. Therefore the calculations presented in the subsequent paper were performed according to the CN-scheme. In the absence of an external series resistance, however, the above condition is not fulfilled. In this case an L-stable (strongly absolutely stable) scheme must be used which provides a stronger damping of the artificial oscillations (cf. Lambert 1973). Thus the computations presented in this paper were done using the L-stable implicit Euler method.

The typical time course of the potential V_m is as follows: fast initial oscillations induced by cable properties; slower changes due to activation and inactivation of

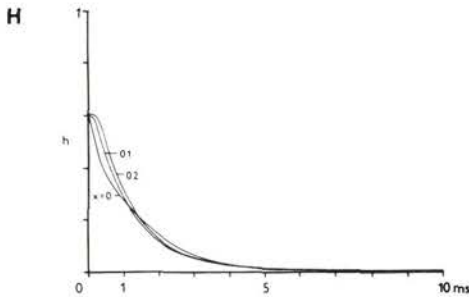
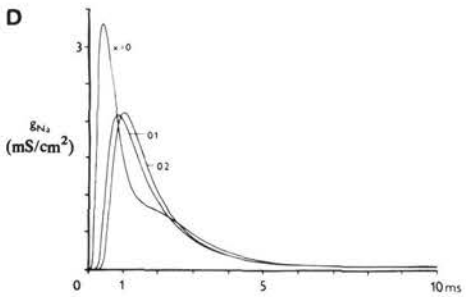
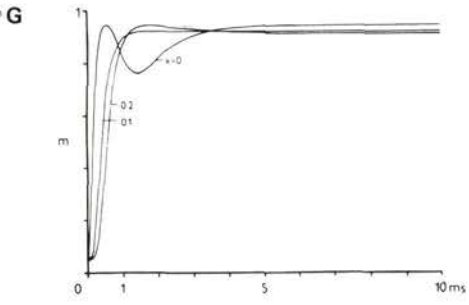
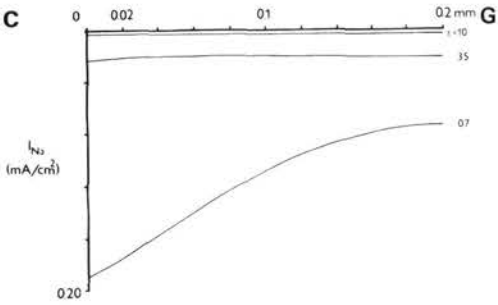
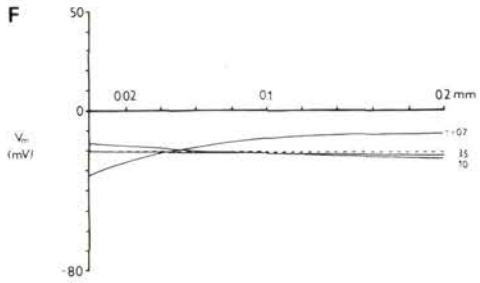
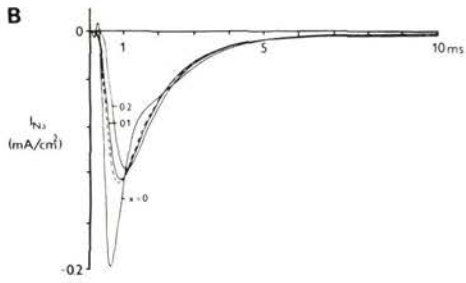
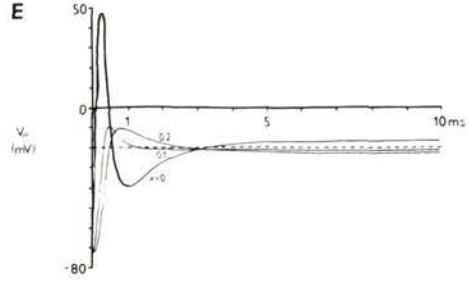
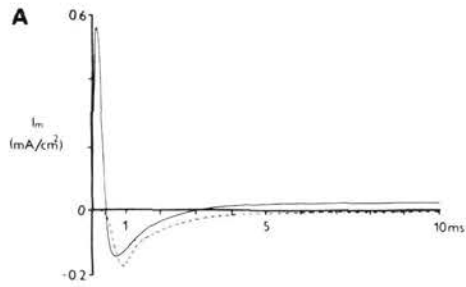
the Na system of the membrane; steady state after several milliseconds. The individual sizes of the time steps were adapted to the time course of the solution and calculated by a step size control algorithm (Grigorieff 1972). The system of nonlinear equations arising in each time step was linearized by Newton's method (one iteration step turned out to be sufficient).

Finally, in each time step a linear system for $(3N+5)$ unknowns is to be solved. The special structure of the matrix allows partial elimination of the unknowns $m_0, \dots, m_N, h_0, \dots, h_N$, so that the order of the matrix reduces to $(N+3)$. The system is very sparse and solved efficiently by the sparse matrix solver MA28 from the Harwell Library (Hopper 1978) which is much faster than the usual (unmodified) Gaussian elimination. In all simulations we obtained sufficiently accurate results with $N=16$ and an error bound for V_m of 1 mV in the step size control algorithm. The program was written in FORTRAN and run on an IBM/370-158 computer. The CPU-times were in the range of 2-5 seconds.

Results

The following clamp simulations are concerned with a simplified system in which the external series resistance (R_s) is set zero. This case may be considered as representative of isolated fibers or fiber bundles with wide intercellular clefts (e.g. rabbit Purkinje strands; Sommer and Johnson 1968). In the absence of a series resistance, voltage and current distribution along the fiber are determined by cable properties only. Fig. 4 illustrates the response of an active fiber to a command pulse of 52 mV amplitude. As the excitable membrane is depolarized, Na conductance rapidly increases and a transient inward current flows across the membrane. The time course of clamp current exhibits three phases (Fig. 4A), a short (about 0.4 ms) period of outward current (similar to the transient phase of clamp current in Fig. 3D) which mainly represents the charging process of the membrane, an

Fig. 4. Voltage clamp response of an active, isolated fiber ($\bar{g}_{Na} = 10$, $g_K = 0.5$ mS/cm²; $R_i = 200$ Ω cm; $R_s = 0$; $G = 50$; $\tau = 0.05$, $\tau_1 = 0.1$, $\tau_2 = 0.01$ ms). Clamp step from resting potential (-72 mV) to -20 mV applied at zero time. (A) Clamp current (expressed as current per cm² of membrane in the test node, I_m ; solid line), corrected inward current (dashed line), and Na inward current of the H—H model (dotted line) during a 52-mV step depolarization. (B) Time course of Na⁺ current across the membrane at the I-end ($x = 0$), in the middle of the fiber ($x = 0.1$ mm), and at the V-end ($x = 0.2$ mm). The dashed curve represents the mean Na current density of the test node. (C) Profile of Na current density along the cable at three times (0.7, 3.5, and 10 ms after onset of the clamp). (D) Na conductance as function of time; the same positions as in (B). (E) and (F) Time course and longitudinal profile of transmembrane potential, respectively; the same arrangement as in (B) and (C). The horizontal interrupted lines represent the command potential, $E_c = -20$ mV. (G) and (H) Na activation and inactivation parameters, m and h , as functions of time; the same positions as before.



inward current wave reflecting activation and inactivation of the Na system, and a phase of outward current which is mainly carried by K ions and attains a steady level at the end of the clamp. A separate calculation of the current flowing through the shunt pathways (R_{sh}) shows that the contribution of the leakage current to the clamp current, I , remains in the order of 5 % throughout the clamp. In a first approximation, then, the clamp current may be considered to represent the total (ionic plus capacitive) current of the nodal membrane. Qualitatively, the current curve resembles what one would expect from a proper space clamp; in particular, it does not exhibit any "notches". As an attempt to separate the Na current from the other current components, a second calculation was done in which \bar{g}_{Na} was set zero and the related membrane current was subtracted from the original current curve. (This is similar to the procedure used in voltage clamp experiments on natural fibers, namely, a comparison of clamp current records in Na-containing and Na-free solutions.) The "corrected" inward current obtained in this way still contains some non-Na current (see below). It has a similar time course as the control current of a single membrane patch under ideal clamp conditions (apart from a delay in the turn-on process) but is distinctly larger in size, the peak values being 168 and 115 $\mu\text{A}/\text{cm}^2$, respectively.

To study the fiber response in more detail, let us consider the current and voltage distribution along the test node as it varies with distance and time. When a step command is applied to the control amplifier and current is injected into the fiber at $x=0$, the related changes in transmembrane current, voltage, and conductance spread along the test node like a decremting wave. Assuming that the membrane potential at the V-end (V_d) is kept near the command level, the time course of membrane current at $x=d$ would reflect the true H-H current at this potential. However, larger currents are recorded from cable segments outside the V-end ($x < d$), with a maximum at $x=0$. This effect is clearly seen in Fig. 4B and C where the Na current densities are shown as functions of time at three positions and as functions of distance at three times, respectively. In Fig. 4B, peak inward current at $x=0$ exceeds that at $x=d$ by about 70 %. The delay time between the two peaks is approximately 0.4 ms which means an overall propagation velocity of $0.2 \text{ mm}/0.4 \text{ ms} = 0.5 \text{ m/s}$. The normalized sum of the Na currents from all segments (dashed curve) yields a peak value of 127 $\mu\text{A}/\text{cm}^2$. This is slightly more than the control value (115 $\mu\text{A}/\text{cm}^2$). Larger peak values seen in the records of clamp current and "corrected" inward current (Fig. 4A) are due to a superposition of ionic with capacitive currents which mainly arise from the segments near the I-end of the fiber.

The time courses of membrane potential at three positions are illustrated in Fig. 4E. The initial transients are similar to those seen with the passive cable (Fig. 3C). After activation of the Na system, a time-dependent voltage gradient develops along the fiber such that V_0 deviates from V_d in the hyperpolarizing

direction (Fig. 4F). The deviation reaches a maximum of 28 mV about 1 ms after onset of the clamp and decreases as the Na system is inactivated. During steady outward current flow the voltage gradient is in the opposite direction. The gradient is steeper during early inward than during outward current since the transient increase of Na conductance (Fig. 4D) leads to an increase of the "electrotonic length" of the test node. An almost uniform polarization of the membrane is attained only at a singular time, namely, at the transition from inward to outward current. Fig. 4G and H show the H-H variables m and h as they vary with time. Activation reaches a level of about 90%. The curves are monotonical in shape, except for the activation curve at $x=0$ which exhibits a transient depression after an initial peak. This deformation is the consequence of the hyperpolarization of membrane potential seen in Fig. 4E.

The potential distribution along the fiber is complicated by the fact that the membrane potential at the recording point ($x=d$) is not under full control (in contrast to the simplifying assumption made above) but deviates from the command potential by up to 9.5 (2.4) mV in the depolarizing (hyperpolarizing) direction during the phase of inward (outward) current. This error is mainly due to the low gain of the control amplifier ($G=50$). Assuming that the control amplifier operates under quasi-steady conditions when the initial phase of membrane charging is over, and neglecting the effect of the compensating amplifier, the feedback signal E_f equals $V_d R_{sh}/(R_{sh} + R_{ax}) = V_d 20/21$ and the potential V_d is correlated to the command signal E_c and the output voltage Φ by

$$(E_c - V_d 20/21)50 = \Phi \quad \text{or} \quad V_d = E_c 21/20 - \Phi 21/1000 \quad (5a)$$

Since the variation in Φ during clamp has a similar time course as the clamp current, V_d undergoes a fluctuation around $E_c 21/20 = -21$ mV which is roughly proportional and opposite to the instantaneous value of I . The general effect of the fluctuation of V_d is to decrease the driving force for membrane current, thereby counteracting the cable effect which per se tends to increase the driving force along the test node (cf. Fig. 4F).

Fig. 5A shows a family of membrane currents, $I_m(t)$, associated with command steps to potentials between -50 and 50 mV. I_m is taken as clamp current I divided by the area of nodal membrane. At $E_c = -50$ mV a small inward current related to activation of the Na system (peak at about 1.3 ms) is preceded by a larger downward deflection which is part of a damped oscillation at the beginning of the clamp (cf. current curve in Fig. 3D). With increasing depolarization the Na inward current wave is shifted to earlier times so that initial oscillation and Na current fuse more and more. (The term "Na current" is used, in a more general sense, for the total membrane current flowing during the phase of transient Na conductance increase.) The relative contribution of Na current to the apparent inward current wave is maximal at depolarizations between -20 and 0 mV and decreases with

strong depolarizations. When the inward current is corrected by the subtraction procedure described above, the peak current-voltage relation shown in Fig. 5B is obtained. At any level of depolarization below $E_{Na} = 43$ mV, the "corrected" inward current of the fiber is larger than the control value. Interception of the current-voltage curve with the voltage axis is not well defined since the subtraction procedure yields small, biphasic currents at potentials above E_{Na} . Extrapolation of the ascending limb results in an apparent reversal potential of about 50 mV.

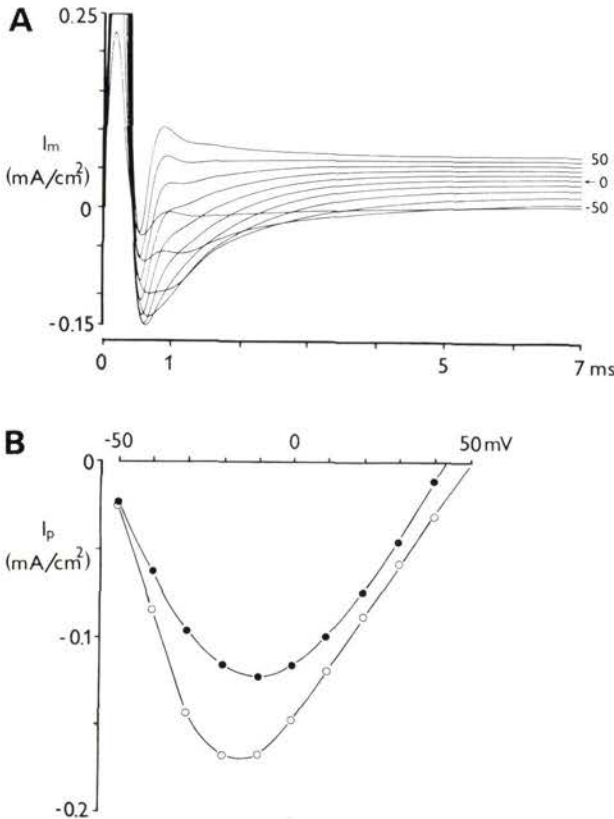


Fig. 5. (A) Simulation of membrane currents of a "voltage-clamped" active fiber at different levels of depolarization. Numbers at the curves indicate the absolute command potential (in millivolts); the command signal was varied in 10 mV steps. The same parameters as in Fig. 4. (B) Peak inward current-voltage diagrams for the corrected membrane current of the fiber (open symbols) and for the Na current of a free patch of membrane (filled symbols).

The results described so far have many features in common with the voltage clamp simulations of Moore et al. (1975) for squid and lobster axons, in particular concerning development of a longitudinal voltage gradient in the repolarizing direction during transient inward current flow. A typical artefact observed by

Moore et al. is a deformation of Na current by notches or, in extreme cases, the occurrence of two separate inward current waves (cf. their Fig. 3C). This error is not seen in the clamp current record of Fig. 4A; a precursor, however, is the non-monotonical shape of the m-curve at the I-end of the test node (Fig. 4G). The deformation becomes more accentuated when higher values of Na conductance are considered. In Fig. 6 the clamp response of an active fiber with $\bar{g}_{Na} = 50$ rather than

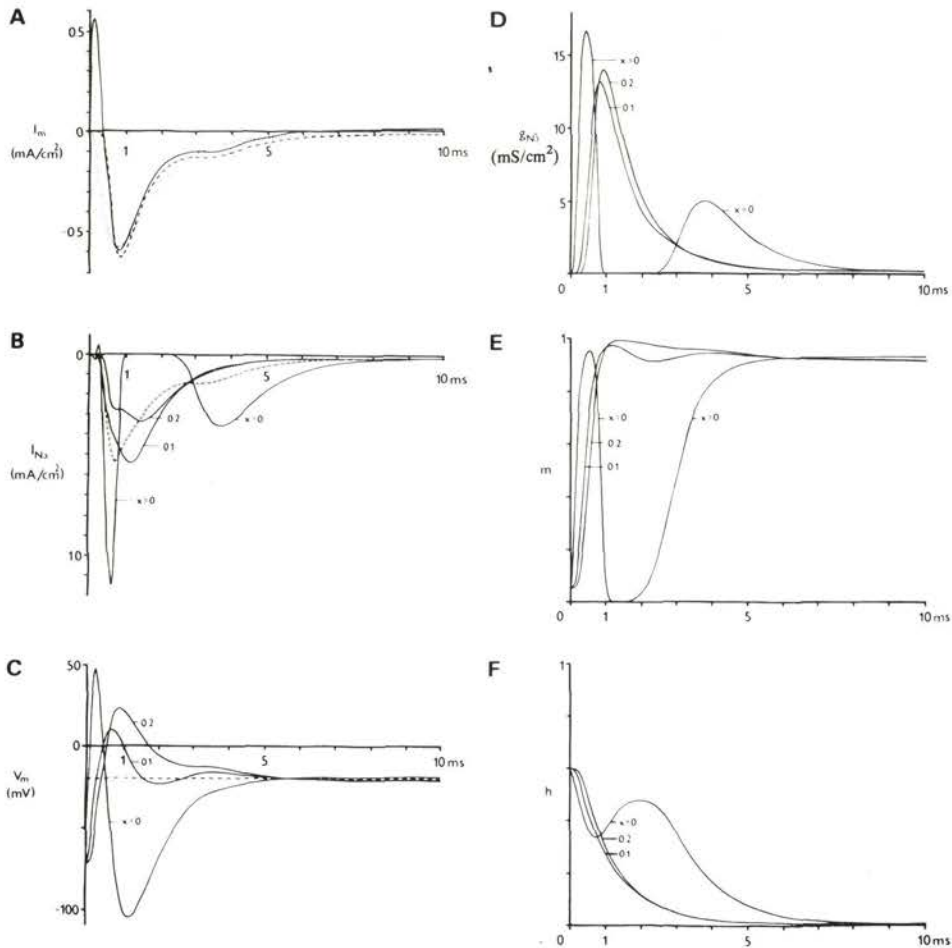


Fig. 6. Results of simulation of a voltage clamp for a fiber with a maximum Na conductance, \bar{g}_{Na} , of 50 mS/cm²; all other parameters of the fiber and the voltage clamp circuit were the same as those used for Fig. 4. Clamp step from -72 to -20 mV. (A) Total membrane current; (B) Na⁺ current, (C) membrane potential, (D) Na conductance, (E) activation variable *m*, and (F) inactivation variable *h* at three positions as functions of time.

10 mS/cm² is illustrated. The voltage deviations during inward current flow (C) are of similar nature as those in Fig. 4 but of enormous size. Voltage control at the V-end is very poor and the time course of V_d resembles the wave form of a free-running action potential (cf. Kootsey and Johnson 1972, Fig. 2) with a peak of 22 mV. The voltage gradient along the fiber is so steep that for a short period the I-end is repolarized to potentials negative to the resting level. This causes an abrupt deactivation of the Na system at the left border of the test node and the inward current wave is cut off after a few tenths of a millisecond (B). The related changes of the H-H variables m and h are shown in (E) and (F), respectively. At $x=0$, the activation variable m , after an initial increase, falls to zero level and remains at zero

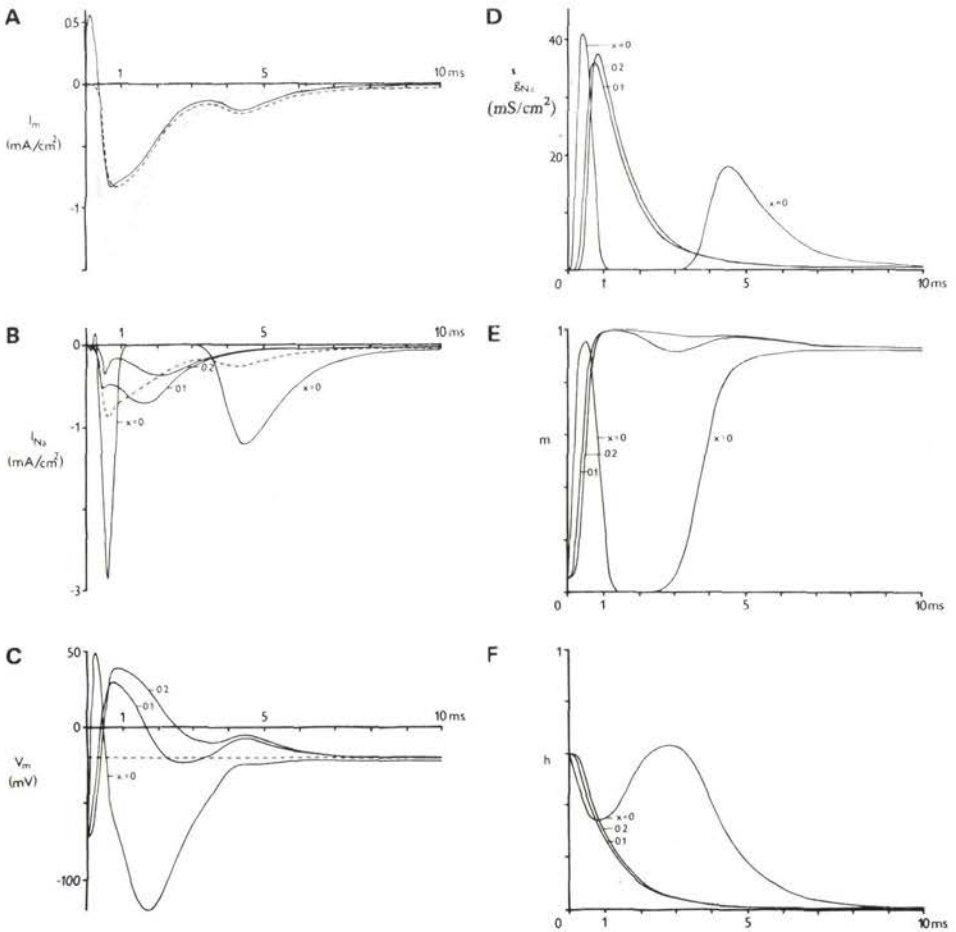


Fig. 7. Results of simulation of voltage clamp for a fiber with $\bar{g}_{Na} = 120$ mS/cm². The same parameters and arrangement of the curves as in Fig. 6.

for about half a millisecond while the inactivation variable h , after an initial decrease, rises to a level which is about 80 % of its resting value. Thus Na conductance increases (D) and a second inward current is generated at the I-end of the test node (B) when the membrane depolarizes again. This effect is also seen, in an attenuated fashion, in the total membrane current record (A). In spite of the large nonuniformities of voltage and current distribution, peak value and time to peak of total membrane current are close to the ideal H-H values.

Fig. 7 shows an analogous computation with $\bar{g}_{Na} = 120 \text{ mS/cm}^2$. Cable complications are even more pronounced than before. In this case the hyperpolarization of the I-end (which brings Na conductance to zero level) and the excess depolarization of the V-end (which means a reduced driving force for Na ions) are so strong that early inward current recorded from the total membrane of the test node is distinctly smaller than the control value. Na current flow at the I-end is mainly in the form of a second inward current wave. A distinct second inward current is also seen in the total membrane current record.

Discussion

The influence of longitudinal resistance of a fibre on membrane current measurements in a double sucrose gap voltage clamp arrangement was demonstrated by Moore et al. (1975) using a model for squid and lobster giant axons. These authors have shown that a good voltage uniformity can be achieved when the length of the test node is smaller than, or equal to, the diameter of the fiber but voltage inhomogeneities occur as the node length/diameter ratio, i.e. the axial resistance of the fiber increases. Since the sites of current injection and voltage control are separated by the full length of the test node, a clamp current that is appropriate for the monitored end causes a voltage gradient along the internal pathway, i.e. deviations of the transmembrane potential from the command signal in the fiber segments away from the V-end. The potential shift is away from the equilibrium potential of the membrane and increases with increasing distance from the controlled segment. Assuming a time and voltage independent membrane conductance, current density outside the V-end will be larger than the corresponding current recorded with an ideal space clamp. The effect is more complex when membrane conductance varies with voltage and time as does the Na conductance. When the Na system of the membrane is activated by a command pulse below the Na equilibrium potential, E_{Na} , and current is withdrawn from the test node the voltage deviation is in the hyperpolarizing direction. The hyperpolarization has a dual effect on Na current since it increases the driving force for transmembrane inward current, but may reduce the Na conductance increase compared to the V-end. In the computations presented by Moore et al. (1975; Fig. 3B, C) the result is a depression of Na current at the I-end of the fiber. In the case of a large voltage

gradient the turn-off of hyperpolarization may give rise to a second inward current wave.

The present paper is an extension of the above work and is concerned with voltage clamp simulations for thin fibers where the node length/diameter ratio is far above unity. A much smaller fiber diameter leads to pronounced cable complications. As expected we observed a distinct voltage gradient during the phase of Na inward current. Since the internal pathway is taken as a pure ohmic resistance the voltage gradient per se is independent of frequency. In our model, however, frequency-dependent phenomena play an important role and modify the effect of a longitudinal voltage gradient on the Na system. The main point is that a spread of polarization from the I-end to the V-end takes appreciable time. This implies a strong tendency of the circuit to oscillate with relatively low frequencies in response to a step input (cf. Kootsey and Johnson 1972). In our arrangement the transient voltage response is reduced to an underdamped oscillation (with a log decrement of 3–4 and a damping coefficient of $\approx 7/\text{ms}$, cf. Fig. 3C) by the use of a low-gain control amplifier and the insertion of a phase lead into the feedback circuit. When a depolarizing command pulse below E_{Na} is applied the primary response of the fiber is a voltage overshoot at the I-end of the test node (cf. Fig. 4E) lasting some tenths of a millisecond. (This phase is missing in the model of Moore et al. 1975.) The voltage overshoot is sufficient to strongly activate the Na system (that is, the parameter m tends to unity). This takes place before activation reaches the V-end and the typical hyperpolarization develops at the I-end. During hyperpolarization, then, Na conductance is high first and quickly declines thereafter (as m tends to zero). The result of a high Na conductance, combined with a high driving force, is a large but short-lasting inflow of Na ions at the I-end of the fiber, with a peak current density that is distinctly larger than peak I_{Na} under ideal voltage clamp conditions (cf. Fig. 4B, 6B, 7B).

Not only the I-end but also the V-end of the test node is affected by cable complications. Because of the low gain of the control amplifier voltage control is imperfect even at the site of voltage monitoring. During Na activation the membrane potential of the V-end overshoots the command level and swings towards the Na equilibrium potential, E_{Na} . At this time the axial voltage gradient is between a depolarization (relative to E_c) at the V-end and a hyperpolarization at the I-end (cf. the voltage profile shown in Fig. 4F). The higher the Na conductance, \bar{g}_{Na} , the larger the depolarization at the V-end. With $\bar{g}_{\text{Na}} = 10 \text{ mS/cm}^2$, the overshoot is in the order of 10 mV (Fig. 4E); with $\bar{g}_{\text{Na}} = 120 \text{ mS/cm}^2$, peak depolarization comes close to the Na equilibrium potential (Fig. 7C). The voltage overshoot decreases the driving force for Na current but favors activation of Na conductance. As a result, peak Na current density at $x = d$ is almost equal to, or smaller than, the control value (Fig. 4A, B and 7A, B).

Concerning the total current recorded from the test node, the deviation from

the ideal configuration is surprisingly small. This is because the errors arising from the individual segments abolish each other to some extent. Size and direction of the resulting error vary with varying values of Na conductance, \bar{g}_{Na} . In the case of a low \bar{g}_{Na} peak value of total Na inward current is slightly larger than the control (Fig. 4) while it is smaller than the control at a high Na conductance (Fig. 7). An example for an almost complete abolishment of the individual errors is shown in Fig. 6 where the clamp current record (apart from a minor distortion of Na current decay by a second activation) looks quite similar to the control one.

In a simplifying view, the records presented in this paper may be characterized as follows. The basic effect of axial resistivity on voltage clamp measurements in a double sucrose gap is a voltage gradient along the fiber, with the consequence that membrane current, in general, would be measured too large. This effect, however, is complicated by a poor voltage control at the monitored end of the test node. In a formal sense, the deviation of the monitored potential (V_d) from the command signal is of the same kind as if the membrane plus a fictitious series resistance were kept under full control (cf. Haas et al. 1986). In general, a series resistance leads to a situation where membrane current is measured too small. Thus the deviation of actual membrane current measurement from the ideal configuration may be understood as the result of two opposing errors.

Table 1. Symbols and Definitions

a	fiber radius (cm)
d	width of test node (cm)
b	width of sucrose gap (cm)
R_i	internal resistivity (Ωcm)
r_i	internal resistance per unit fiber length = $R_i/\pi a^2$ (Ω/cm)
R_{ax}	internal resistance in sucrose gap = br_i (Ω)
R_{sh}	sucrose gap leakage resistance (Ω)
q	short-circuiting factor = $R_{\text{ax}}/(R_{\text{sh}} + R_{\text{ax}})$
R_p	over-all parallel resistance of sucrose gap = $R_{\text{sh}}R_{\text{ax}}/(R_{\text{sh}} + R_{\text{ax}})$ (Ω)
R_m	resting membrane chord resistance x unit area of fiber surface (Ωcm^2)
r_m	membrane resistance x unit length = $R_m/2\pi a$ (Ωcm)
C_m	membrane capacitance per unit area (F/cm^2)
τ_m	membrane time constant = $R_m C_m$ (s)
R_s	resistance in series with membrane in test compartment (Ω)
λ	length constant of fiber in central pool = $\sqrt{r_m/r_i}$ (cm)
V_m	absolute membrane potential in test compartment (V) (inside minus outside potential)
I	total current delivered by control amplifier (A)

I_m	membrane current density in test node (A/cm ²)
I_{ion}	membrane ionic current density (A/cm ²)
E	potential of voltage pool with respect to ground (V)
E_f	feedback signal (V)
E_c	command signal (V)
G	low-frequency open loop gain of control amplifier
τ	time constants of control amplifier (s)
Φ	output voltage of control amplifier (V)
τ_1, τ_2	time constants of input and feedback impedances of compensating amplifier (s)
x	distance along the test node (cm)
t	time after onset of a clamp (s)

Appendix

Nyquist analysis of voltage control

With a passive RC cable as preparation, the voltage clamp circuit of Fig. 2 is converted into a linear, time-invariant network, and the dynamic response of the system to an external signal can be determined by analytical methods. Since the stability problem is most serious in the absence of an external series resistance, analysis will be restricted to the case $R_s = 0$. For simplicity the resting potential and the initial values of Φ , E , and E_f are all set to zero level. Information about stability is available from a polar plot of the sinusoidal open loop transfer function. In Fig. 8 the feedback circuit of Fig. 2 is shown in the form of a block diagram where G_1 , G_2 , and H represent the respective transfer functions for the control amplifier, the preparation (test node and sucrose regions), and the lead network (compensating amplifier). The transfer functions of the two amplifiers are directly obtained by taking the Laplace transforms of eqs. (5) and (6):

$$G_1 = \frac{\Phi}{E_{in}} = \frac{G}{1 + \tau s}; \quad H = \frac{E_f}{E} = \frac{1 + \tau_1 s}{1 + \tau_2 s} \quad (10)$$

The transfer function of the preparation follows from conventional cable theory. For a passive cable with zero resting potential, the ionic current flow across the membrane may be written as V_m/R_m . Thus we have the cable equation (1) in the standard form

$$\lambda^2 \partial^2 V_m / \partial x^2 = \tau_m \partial V_m / \partial t + V_m \quad (1a)$$

which transforms to

$$\lambda^2 d^2 \bar{V}_m / dx^2 = u^2 \bar{V}_m \quad (1b)$$

where $u = \sqrt{1 + \tau_m s}$. Using the boundary conditions (eqs. (2) and (3)) and the auxiliary equations (4) and (7), the transfer function for the preparation comes to

$$G_2 = \frac{\tilde{E}}{\tilde{\Phi}} = \frac{(1 - q)}{(1 + q) \cosh (ud/\lambda) + [ub/\lambda + q\lambda/(ub)] \sinh (ud/\lambda)} \quad (11)$$

G_2 is an even function of u and a single-valued function of s . The singular points of G_2 in the s -plane are first-order poles and correspond to the zeros of the denominator in eq. (11). The poles are given by

$$s_v = -\frac{1 + (y_v \lambda/d)^2}{\tau_m}; \quad v = 1, 2, \dots \quad (12a)$$

where y_v are real numbers defined by the relation

$$\tan y_v = \frac{(1 + q)y_v}{y_v^2 b/d - qd/b} \quad (12b)$$

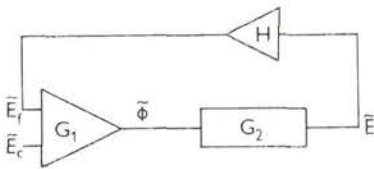


Fig. 8. Scheme of the voltage-clamp circuit, with all quantities in Laplace transform notation.

The poles of G_2 are all located on the negative half of the real axis of the s -plane, the first pole being $s_1 = -1/\tau_m$.

The open loop transfer function is the product of the individual transfer functions, $P(s) = \tilde{E}_t/\tilde{E}_c = G_1 G_2 H(s)$, with $E_{in} = E_c$. By substituting $j\omega$ for s in the expression for $P(s)$ the open loop frequency response is obtained. For $\omega \rightarrow \infty$, $P(j\omega)$ tends to zero. According to the Nyquist criterion, the closed loop system is stable if the polar plot of $P(j\omega)$, with increasing values of ω , does not encircle the point $(-1, 0)$ in the $P(s)$ -plane. In other words, the $P(j\omega)$ -contour must not intersect with the negative real axis at a point left from, or equal to, the $(-1, 0)$ point (for details see DiStefano et al. 1976).

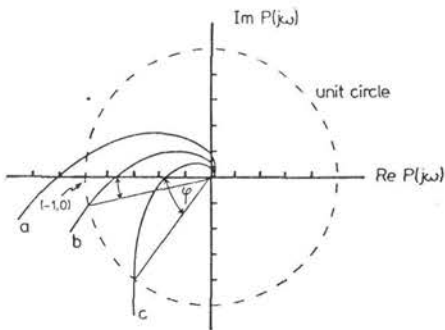


Fig. 9. Nyquist stability plots obtained with different configurations of control amplifier (G , τ) and lead compensation (τ_1 , τ_2). For the numerical values of G , τ , τ_1 and τ_2 used for curves a—c see legend to Fig. 3 A—C. All other parameters were identical in the three calculations ($R_{ab}/R_{ax} = 20$; $R_m = 2\text{ k}\Omega\text{cm}^2$; $R_i = 200\ \Omega\text{cm}$; $\lambda = 0.038\ \text{cm}$; $d = 0.02\ \text{cm}$). The angle φ represents the phase margin.

In Fig. 9 Nyquist plots are used to demonstrate the influence of a lead compensation on the stability of the voltage clamp circuit. The plots are restricted to the mid-frequency range where the curves cross the negative real axis and approach the origin of the $P(s)$ -plane. Parameters used to construct the curves labelled *a*, *b*, and *c* were the same as those employed for the voltage clamp simulations shown in Fig. 3A, B and C, respectively. When the gain of the control amplifier is set to $G = 100$ and a lead network is missing, the system is unstable as indicated by the intersection of curve (*a*) with the real axis at the point $(-1.2, 0)$. The crossover frequency is 1048 Hz which is close to the frequency of increasing oscillation seen in Fig. 3A. After the insertion of a phase lead the Nyquist path remains almost unaffected in the low frequency range (not shown) but is shifted to the right for medium frequencies such that intersection occurs at $(-0.75, 0)$, with a phase crossover frequency of 1620 (*b*). The system is stable and the phase margin amounts to $\approx 13^\circ$. Stability is reflected by the decreasing oscillation in Fig. 3B. With $G = 50$, the relative stability of the system is further increased. Intersection is now at $(-0.34, 0)$ with a crossover frequency of 2070 Hz and the phase margin has expanded to 53° . Increased stability is manifested by the strong, almost critical damping of the initial oscillation seen in Fig. 3 C.

References

- Attwell D., Cohen I. (1977): The voltage clamp of multicellular preparations. *Progr. Biophys. Mol. Biol.* **31**, 201–245
- Beeler G. W., McGuigan J. A. S. (1978): Voltage clamping of multicellular myocardial preparations: Capabilities and limitations of existing methods. *Progr. Biophys. Mol. Biol.* **34**, 219–254
- Crank J., Nicolson P. (1947): A practical method for numerical evaluation of solutions of partial differential equations of the heat conduction type. *Proc. Cambridge Phil. Soc.* **43**, 50–67
- DiStefano III J. J., Stubberud A. R., Williams I. J. (1976): *Theory and Problems of Feedback and Control Systems*. McGraw-Hill, New York
- Fischmeister R., Mentzard D., Vassort G. (1982): Limitations of voltage clamp studies of slow inward current using the double sucrose gap. *Gen. Physiol. Biophys.* **1**, 319–348
- Grigorieff R. D. (1972): *Numerik gewöhnlicher Differentialgleichungen*, Vol. 1. Teubner, Stuttgart
- Haas H. G., Brommundt G. (1980): Influence of intercellular clefts on potential and current distribution in a multifiber preparation. *Biophys. J.* **30**, 327–350
- Haas H. G., Brommundt G., Solchenbach K. (1987): Voltage clamp simulations for multifiber bundles in a double sucrose gap: Radial vs. longitudinal resistance effects. *Gen. Physiol. Biophys.* (in press)
- Haas H. G., Meyer R., Einwächter H. M., Stockem W. (1983): Intercellular coupling in frog heart muscle. Electrophysiological and morphological aspects. *Pflügers Arch.* **399**, 321–335
- Hodgkin A. L., Huxley A. F. (1952): A quantitative description of membrane current and its application to conduction and excitation in nerve. *J. Physiol. (London)* **117**, 500–544
- Hopper M. J. (1978): Harwell Subroutine Library, a Catalogue of Subroutines. AERE-R 9185, Harwell
- Johnson E. A., Lieberman M. (1971): Heart: excitation and contraction. *Annu. Rev. Physiol.* **33**, 479–532

- Julian F. J., Moore J. W., Goldman D. E. (1962a): Membrane potentials of the lobster giant axon obtained by use of the sucrose-gap technique. *J. Gen. Physiol.* **45**, 1195—1216
- Julian F. J., Moore J. W., Goldman D. E. (1962b): Current-voltage relations in the lobster giant axon membrane under voltage clamp conditions. *J. Gen. Physiol.* **45**, 1217—1238
- Kootsey J. M., Johnson E. A. (1972): Voltage clamp of cardiac muscle. A theoretical analysis of early currents in the single sucrose gap. *Biophys. J.* **12**, 1496—1508
- Lambert J. D. (1973): *Computational Methods in Ordinary Differential Equations*. John Wiley and Sons, Inc., New York
- McGuigan J. A. S. (1974): Some limitations of the double sucrose gap, and its use in a study of the slow outward current in mammalian ventricular muscle. *J. Physiol. (London)* **240**, 775—806
- Moore J. W., Ramón F., Joyner R. W. (1975): Axon voltage-clamp simulations. II. Double sucrose-gap method. *Biophys. J.* **15**, 25—35
- Ramón F., Anderson N., Joyner R. W., Moore J. W. (1975): Axon voltage-clamp simulations. IV. A multicellular preparation. *Biophys. J.* **15**, 55—69
- Sommer J. R., Johnson E. A. (1968): Cardiac muscle. A comparative study of Purkinje fibers and ventricular fibers. *J. Cell Biol.* **36**, 497—526
- Tarr M., Trank J. W. (1974): An assessment of the double sucrose-gap voltage clamp technique as applied to frog atrial muscle. *Biophys. J.* **14**, 627—643

Received August 27, 1985/Accepted March 27, 1986